Journal of Applied Physics A

https://www.springer/journal/339

ISSN	Impact Factor
1432-0630	1.604

Applied Physics A (2018) 124:496
https://doi.org/10.1007/s00339-018-1911-z

Applied Physics A
Materials Science & Processing

$CuInTe_2$ thin films synthesis using one-step electrodeposition process: structural, optical, and electrical characterization

O. Meglali[1,2] · A. Bouraiou[2] · N. Attaf[3] · M. S. Aida[4]

Received: 5 February 2018 / Accepted: 13 June 2018

Abstract
Polycrystalline $CuInTe_2$ (CIT) films were grown onto ITO substrate by one-step electrodeposition technique using acidic aqueous solutions. In this study, the influence of the deposition time on CIT films properties was examined using six techniques, the X-ray diffraction, the scanning electron microscopy, the energy dispersive X-ray analysis, the optical transmittance, the Raman spectroscopy and the electrical properties measurements. The thickness of $CuInTe_2$ films increases as the deposition time increases. The X-ray diffraction investigation of the films deposited during 5 and 10 min shows up only a tetragonal $CuInTe_2$ chalcopyrite structure, with a preferred orientation along [112] direction. However, the films deposited during 15 and 20 min exhibits the $CuInTe_2$ chalcopyrite structure as a main phase with In_4Te_3 as additional secondary phase. We have noticed a change in the preferred orientation axis of the prepared films as function of deposition time. The films show the direct allowed band gap and their energy band gap decreased from 1.06 to 0.99 eV as the deposition time increased from 5 to 20 min. Hall effect measurements show that the deposition time changes the conductivity type and films carrier concentration. The electrical conductivity is affected by the variation in the carrier mobility rather than by their concentration. The observed Raman modes in the films match well with those reported for single crystal $CuInTe_2$ in the literature. All Raman spectra show the A_1 mode at 127 cm^{-1} confirming the chalcopyrite crystalline quality of these films.

1 Introduction

Copper indium ditelluride $CuInTe_2$ belongs to the category of I–III–VI_2 ternary chalcopyrite semiconductors and it is one of the available alternatives to silicon. In recent years, the Cu-III-VI_2 group has received considerable attention because of their potential applications in many fields such as, solar energy conversion, visible and IR light-emitting diodes (LED's), non-linear optical devices and spin electronic devices [1]. In particular, solar cells composed of chalcogenide material Cu(In,Ga)Se_2 (CIGS) have shown 21.7% photovoltaic conversion efficiency [2, 3]. However, one of the challenges with this material is the low vapor pressure of selenium. This problem can be avoided by substituting the selenium by the high vapor pressure element tellurium [4]. The highest reported power conversion efficiency with $CuInTe_2$ absorber layer is 5.1% using conventional MBE system [5]. Mise and Nakada has reported highest efficiency of 6.92% for MgF_2/Al/ZnO:Al/ZnO/CdS/$CuIn_3Te_5$/Mo solar cells structure [6]. Lakhe and Chaure have reported a power conversion efficiency of 4.13%, a short current density of 20 mA cm^{-2}, an open circuit voltage of 480 mV and a fill factor of 43% for (FTO/CdS/$CuInTe_2$/Au) solar cell configuration under AM 1.5 irradiation (100 mW cm^{-2}), the $CuInTe_2$ absorption layer in this junction is synthesized by electrodeposition method [7].

$CuInTe_2$ is a direct band gap semiconductor; it has an energy gap between 0.96 and 1.06 eV at room temperature. This gap is very close to the range of optimum solar energy conversion [8, 9]. It has large absorption coefficient ($\alpha \approx 10^4 - 10^5\,cm^{-1}$) and exhibits favorable radiation stability. Therefore, CIT is a potential candidate for application as an absorber layer in hetero-junction or multi-junction devices (bottom cells of the tandem solar cells) with other I–III–VI_2 semiconductors and it can be prepared as both p

✉ A. Bouraiou
a_bouraiou@yahoo.fr

1 Faculty of Sciences, Mohamed Boudiaf University, 28000 M'sila, Algeria

2 Materials Science and Informatics Laboratory, Ziane Achour University, 17000 Djelfa, Algeria

3 Thin Films and Interfaces Laboratory, Department of Physics, Mentouri University, 25000 Constantine, Algeria

4 Department of Physics, King Abdulaziz University, Jeddah, Kingdom of Saudi Arabia

Published online: 18 June 2018

and n types conduction [10]. $CuInTe_2$ films have been grown using several techniques, including flash evaporation [11], electrodeposition [4, 7, 10, 12], pulse laser deposition [13], etc. Electrodeposition as a method for $CuInTe_2$ thin film preparation has many advantages over other physical and chemical deposition techniques; it is easy to carry out, low cost and safe. These advantages are highly desired in the research in thin films fabrication.

In this work we present the results of one-step electrodeposition process of $CuInTe_2$ films. The films were deposited onto ITO-coated glass substrates from solutions containing $CuCl_2$, $InCl_3$, TeO_2 and HCl precursors. The X-ray diffraction (XRD) and scanning electron microscope (SEM) were used for analyzing the films structure. The energy-dispersive X-ray analysis (EDAX) was used to identify the composition of the films. The optical transmission, Raman spectroscopy and Hall effect measurements were used to investigate the optical and the electrical properties of the films.

2 Experimental details

Copper indium telluride films were deposited using electrodeposition technique with a simple two electrodes cell configuration. The counter electrode was a platinum sheet. The conductive indium tin oxide (ITO) layer coating high glass substrates (area 5 mm × 15 mm) were used as working electrode (cathode). Film growth process is detailed in paper [14].

A mixture of 10 mM $CuCl_2$, 20 mM $InCl_3$ and 20 mM TeO_2 powder dissolved in distilled deionized water was used as starting solution. The electrolyte pH was adjusted to 2.6. The starting powders used were of 99.99% purity. Deposition was carried out at a room temperature. The as-deposited films were annealed under vacuum at temperature of 300 °C during 30 min.

The films thicknesses were determined by means of Dektak ST. The films crystalline structure was analyzed by means of X-ray diffractometer using CuK_α radiation of wavelength $\lambda = 1.5418$ Å. The crystallite size C_s, was estimated from the full-width at half maximum (FWHM) of the diffraction peak using Scherr's formula [15].

$$C_s = \frac{0.9\lambda}{\beta \cos\theta}, \quad (1)$$

where β and θ (in radian) are respectively the full-width at half maximum corrected and the position of the main peak of the X-ray diffraction spectrum.

The film surface morphology was investigated by scanning electron microscopy (SEM) operating at an accelerating voltage of 15 kV. Composition of the films was estimated by EDAX connected to a SEM. The films optical band gaps at room temperature were determined from the optical transmission measurement using a double-beam Shimadzu UV–Vis–IR spectrophotometer in the wavelength range of 350–1500 nm.

Films electrical resistivity, conductivity type, carrier concentration, and carrier mobility are measured using four point probe method and Hall effect apparatus.

3 Results and discussion

The variations of the films thickness and the growth rate versus the deposition time are shown in Fig. 1. As can be seen, we distinguish two stages (I and II). In stage I; for a deposition time less than 900 s, the films thickness variation is almost linearly related to the deposition time; when the deposition time rises from 300 to 900 s, the films thickness increases from (1.530 ∓ 0.021) to (1.924 ∓ 0.015) µm, however, the growth rate is significantly decreasing (from $5.100 \mp 0.069 \times 10^{-3}$ to $2.138 \mp 0.016 \times 10^{-3}$ µm s^{-1}). In the second stage; for a deposition time greater than 900 s, the films thickness is saturated and the decrease in the growth rate is less rapid. This is due to the fact that at longer deposition time there are fewer free ions of Cu^{2+}, In^{3+} and Te^{4+} in the electrolytic solution to accelerate the growth.

X-ray diffraction analysis was carried out to identify the structure and phases of the investigated thin films. Figure 2a–d shows the X-ray diffraction patterns of the Cu–In–Te annealing films as a function of deposition time (a: 5, b: 10, c: 15 and d: 20 min). The inset of these figures show the X-ray diffraction scans reflecting only the sections of the scan between 23.5° and 26°.

The diffraction peaks identified from the ITO are marked with open circle sign. We found that, after annealing the as-deposited films at 300 °C during 30 min, the ITO substrates

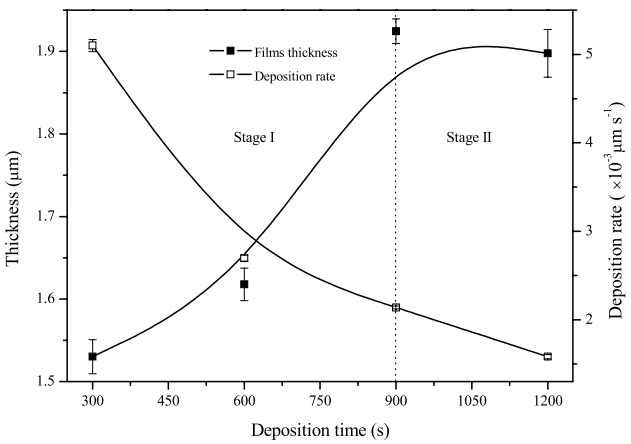

Fig. 1 The films thickness and the growth rate versus the deposition time

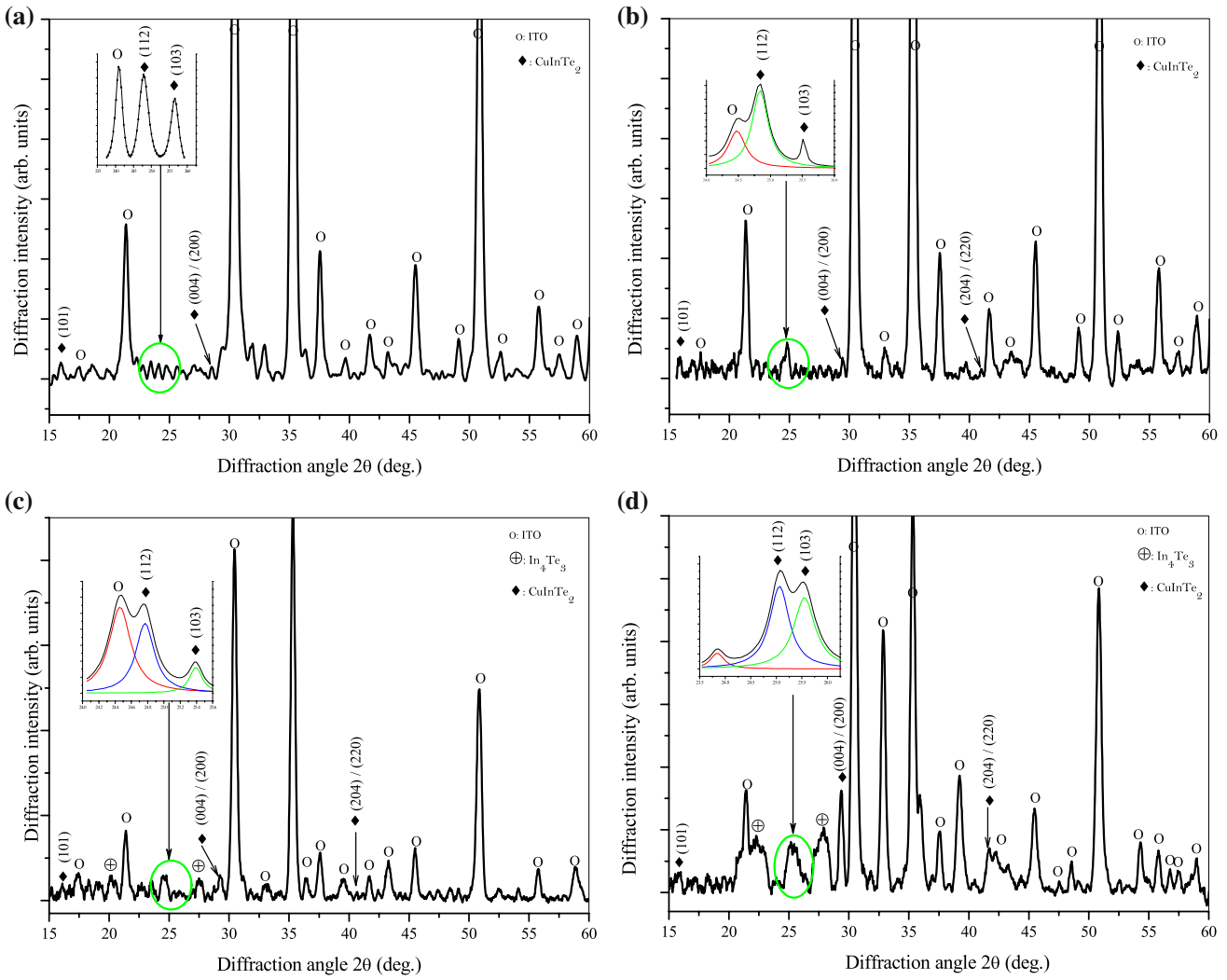

Fig. 2 X-ray diffraction patterns of $CuInTe_2$ deposited on ITO-coated glass substrate after annealing under vacuum at 300 °C during 30 min related to different deposition time: **a** 5, **b** 10, **c** 15 and d 20 min. The inset of these figures show the X-ray diffraction scans reflecting only the sections of the scan 23.5° and 26°, the black line represent the overall fit, the red, blue and green lines denote the individual Lorentzian fit marked as open circle, (112) and (103)

keep their initial crystalline structure and all the elaborated films are polycrystalline.

As can be seen, the films diffraction pattern contains the peaks located at $2\theta \approx 15.92°$, 24.76°, 25.55°, 29.33° and 41.59° (marked by solid diamond symbol in XRD diagram). All these peaks correspond to most intensive peaks for $CuInTe_2$ phase (JCPDS#82-0450) in its tetragonal chalcopyrite structure and with space group of $I\bar{4}2d$. They correspond, respectively, to the (101), (112), (103), (004)/(200) and (204)/(220) planes.

In addition to $CuInTe_2$ reflection peaks, the diffraction pattern of films deposited at 15 and 20 min, shows additional peaks situated at $2\theta \approx 20.05°$, 22.18° and 27.89° (marked by + center circle in XRD diagram), these new peaks are attributed to (101), (320) and (311) planes of In_4Te_3 binary compounds (JCPDS#83-0040). The intensities of these peaks increase with the deposition time, indicating that the amount of In_4Te_3 increases. The In_4Te_3 binary phase is generated by the reaction between the indium cation and H_2Te phase according to the following chemical equation:

$$4In^{3+} + 3H_2Te \rightarrow In_4Te_3 + 6H^+. \quad (2)$$

According to the Pourbaix-type diagram, the H_2Te is generated from the reduction of copper telluride [10]. Note that, in the presence of $HTeO_2^+$, Cu^{2+} and In^{3+}, H_2Te is thermodynamically unstable [4].

The appearance of a secondary phase in the two later films indicates the competitive formation of In_4Te_3 second phase and $CuInTe_2$ material. Many authors have reported the appearance of binaries phases with $CuInTe_2$. Mise et al.

[16] and Lakhe et al. [7] reported that a secondary phase of In_4Te_3 was segregated in the Cu–In–Te based thin films grown, respectively, by co-evaporation and electrodeposition methods. Boustani et al. [17] observed the additional peaks attributed to binary phase of In_2Te_3 in $CuInTe_2$ films prepared by flash evaporation.

To estimate the films preferential orientation, the ratio of (112) diffraction peak intensity was calculated. For films deposited at 5 and 10 min the calculated ratio of (112) peak were, respectively, 0.56 and 0.52. The ratio of (004)/(200) peak were, respectively, 0.54 and 0.79 for films deposited at 15 and 20 min. This means that the first two films are preferentially oriented along the [112] crystalline direction, but the last two films are preferentially oriented along the [004]/[200]. The [112] orientation is known to be beneficial for lattice matching between $CuInTe_2$ and the I II semiconductors.

The lattice constants a and c are calculated using the following equation:

$$d_{hkl} = \left(\frac{h^2 + k^2}{a^2} + \frac{l^2}{c^2} \right)^{-1/2}, \quad (3)$$

where h, k, and l are the Miller indices and d_{hkl} is the interplanar spacing of the (hkl) peak.

Figure 3 shows the variation of the lattice parameters a and c as a function of the deposition time. The inset of this figure shows the variation of the stoichiometric coefficient $\delta = c/a$ versus the deposition time. It can be seen from Fig. 3 that the parameter c increased with 15 min then levels-off within increasing deposition time of 15–20 min. However, for an increasing in the deposition time from 15 to 20 min, the parameter a deceases from 6.20 to 6.06 Å. The obtained

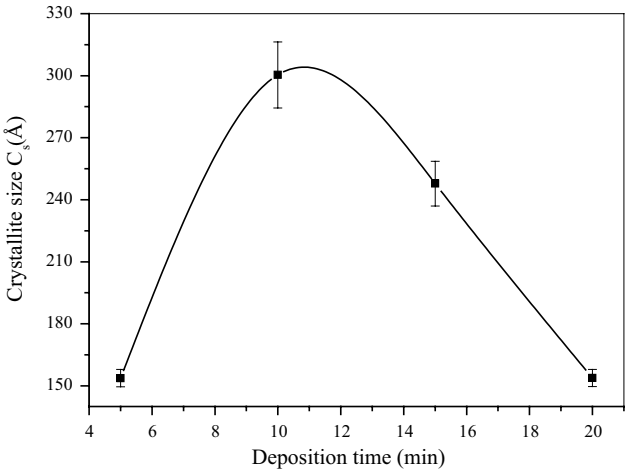

Fig. 4 Variation of crystallite size C_s versus deposition time

values are in good agreement with those reported in the JCPDS card (JCPDS#82-0450) and with literature data [15, 18, 19].

The stoichiometry coefficient δ reflects the deviation from the ideal tetragonal structure, for the $CuInTe_2$ under its ideal tetragonal structure; this ratio is equal to 2.00. It is known that, mostly the optical properties of the I–III–VI_2 chalcopyrites are strongly affected by the compositional deviation from stoichiometry [20]. For our films, the stoichiometry coefficient is almost linearly related to the deposition time (inset of Fig. 3); it varies between 2.02 and 2.10. The films deposited at 5 and 10 min show the smallest deviation from the ideal structure.

From the full-width at half maximum (β) of the main peak of the X-ray diffraction spectrum, one can calculate

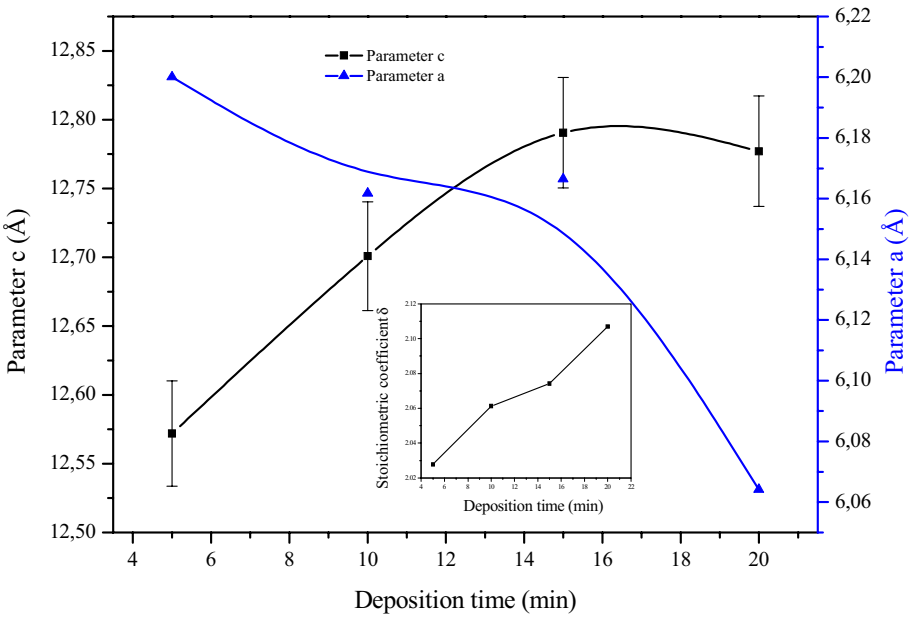

Fig. 3 The variation of the lattice parameters a and c as a function of the deposition time. The inset of this figure shows the variation of the stoichiometric coefficient $\delta = c/a$ versus the deposition time

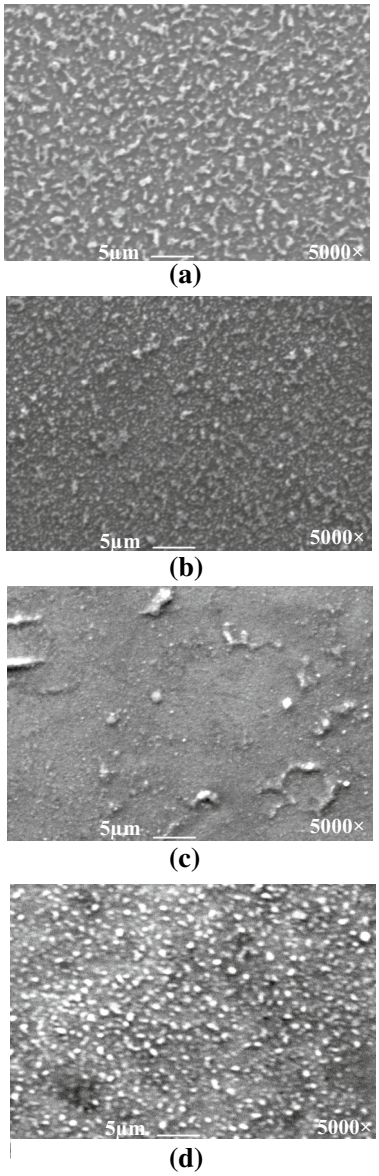

Fig. 5 SEM images of $CuInTe_2$ thin films deposited at **a** 5, **b** 10, **c** 15 and **d** 20 min

the average crystallite size, C_s, using Scherrer's formula (Eq. 1). Before calculating the crystallite size, line broadening due to the equipment was substracted from the peak width. The calculated results are reported as function of the deposition time in Fig. 4. As can be seen, the crystallite size firstly shows an increasing tendency, reaching a maximum value for 10 min and then shows a decreasing tendency with deposition time from 10 to 20 min. Comparing the structural properties of the investigated films we can conclude that the film deposited during 10 min improved the crystallization of the $CuInTe_2$ single phase.

Figure 5a–c shows the morphology of films prepared with different depositions times, (a) 5, (b) 10, (c) 15 and (d) 20 min, respectively. These films show similar polycrystalline morphology, they are dense with a good mechanical adhesion to ITO substrate. The films deposited at 5 and 10 min (Fig. 5a, b) are compact and show a good uniform surface morphology with more dense and homogenously distributed grains. The SEM image of the film deposited during 15 min (Fig. 5c) show a poor film structure with smooth surface formed by dense and small grain size. The surface of the film deposited at 20 min shows well-defined rounded grains of approximately 0.5 µm in size. This difference in the surface morphology reveals that the films show up additional phases as revealed by XRD results that indicated In_4Te_3 binary phase formation in film deposited at 15 and 20 min.

Figure 6a–d shows a representative EDAX pattern of Cu–In–Te thin films. These spectrums show the typical emission lines of copper (CuL), indium (InL) and tellurium (TeL) elements in the investigated energy range. The appearance of silicon (SiK), oxygen (OK) and tin (SnL) peaks comes mainly from the ITO-coated glass substrate.

The optical absorption measurements for the elaborated films show a high absorption coefficient of the order of 10^4 cm^{-1}. The linear nature of the plot of $(\alpha h\nu)^2$ against $(h\nu)$ near the absorption edge (Fig. 7a–d), confirmed that all prepared films are semiconducting material with a direct allowed transition. The energy band gaps are evaluated from the linear extrapolation of $(\alpha h\nu)^2$ values for each film to the $(h\nu)$ axis (Fig. 7a–d). The films grown during 15 and 20 min have relatively higher optical absorption; this is due to the difference in the films thickness and to the presence of the In_4Te_3 phase. We noted also, the absence of a sharp

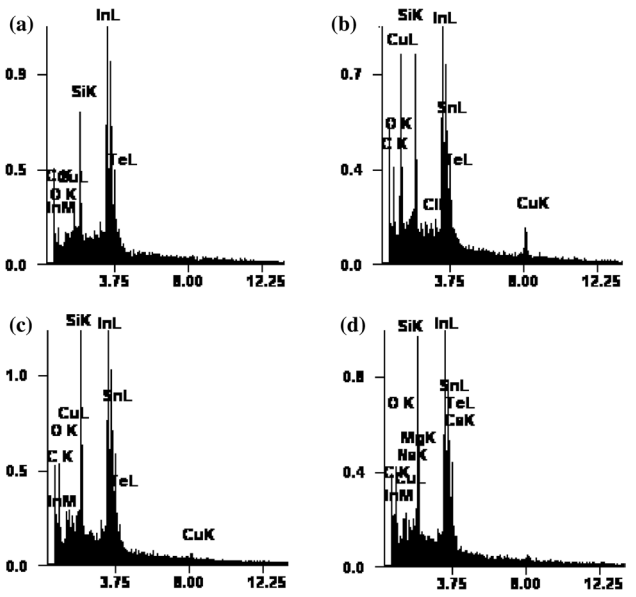

Fig. 6 EDAX patterns of the resulted films for different deposition times **a** 5, **b** 10, **c** 15 and **d** 20 min

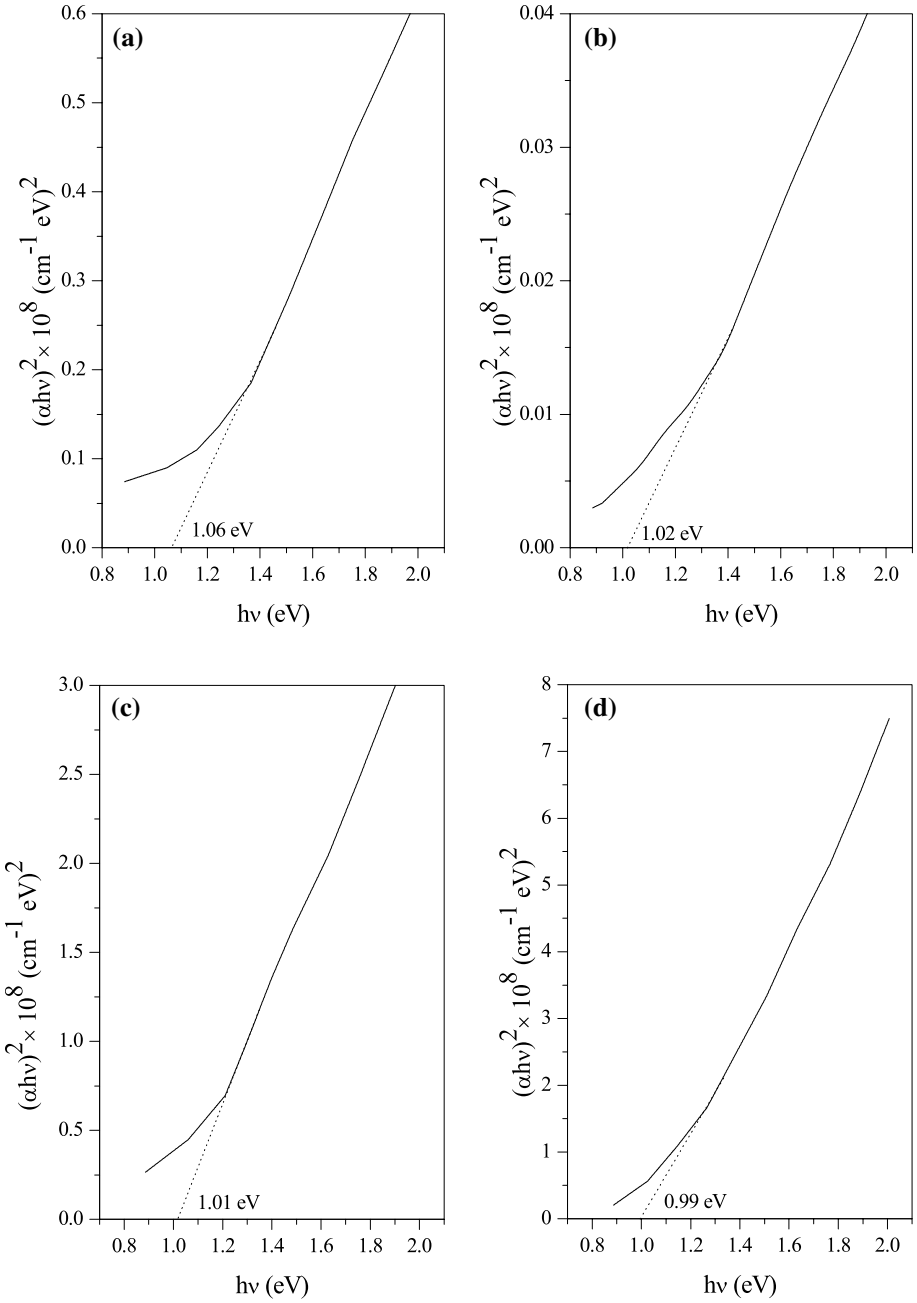

Fig. 7 Dependence of the parameter $(\alpha h\nu)^2$ on radiation energy $(h\nu)$ for different deposition times **a** 5, **b** 10, **c** 15 and **d** 20 min

absorption edge at the photon energy around the E_g, this can be due to the presence of defects levels which were formed by impurities or to the presence of secondary phases.

Figure 8 depicts the variation of the energy band gap versus the deposition time. From this plot, the energy band gap is a decreasing function of the deposition time, the obtained values varied between 0.99 and 1.06 eV. These values fall in the optimum range for the terrestrial solar energy conversion and they are in good agreement with values reported in the literature [21, 22]. Murali et al. [23] have reported that the E_g values vary from 0.98 to 1.02 eV for $CuInTe_2$ deposited using pulse electrodeposition technique.

Electrical resistivity, carrier mobility and carrier concentration were determined in the room temperature by Hall effect and resistivity measurements, the obtained results are reported in Table 1. Only the film deposited during 10 min exhibits p-type conduction with the high holes concentration. Lacruz et al. [24] reported that, $CuInTe_2$ grown from near-stoichiometric compositions exhibits p-type conductivity, this p-type behaviour is caused by tellurium vacancies defect (V_{Te}) which act as acceptors in $CuInTe_2$ [18, 25].

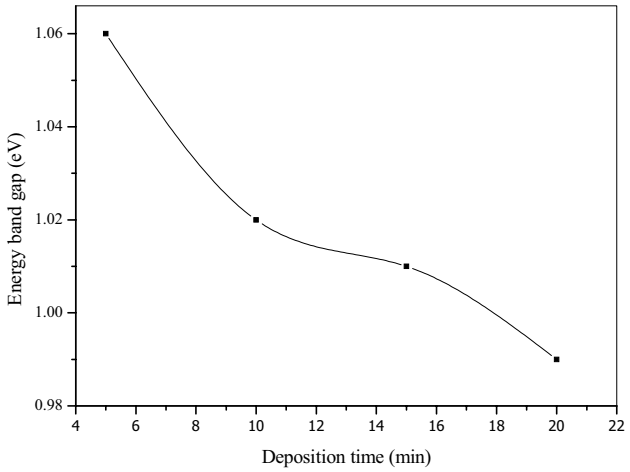

Fig. 8 Variation of the band gap energy E_g versus deposition time

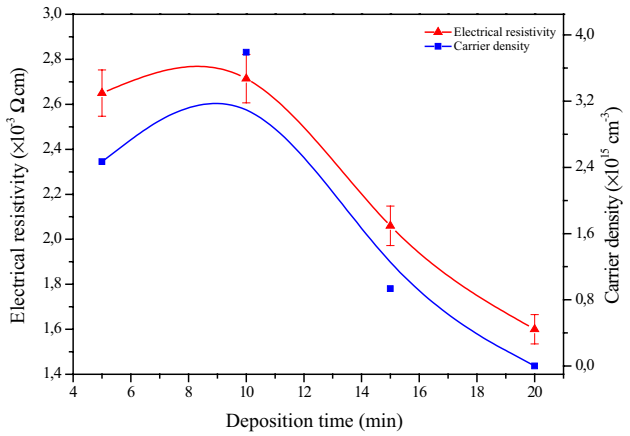

Fig. 9 A plot of the electrical resistivity and the carrier density of $CuInTe_2$ films versus deposition time

The variation of the electrical resistivity and the carrier density with deposition time are shown in Fig. 9. It is observed that the resistivity of the films decreases from $(2.65 \mp 0.10) \times 10^{-3}$ to $(1.60 \mp 0.06) \times 10^{-3}\,\Omega\,\text{cm}$ as the deposition time increases.

It is well known that the electrical resistivity is inversely proportional to the free carrier density and to the carrier mobility; $\rho = 1/e(n\,\mu_n + p\mu_p)$, where n and p (μ_n and μ_p) are, respectively, the electron and hole concentration (and mobility). However, in this work, we have observed that the electrical resistivity evolution has the same shape as the carrier density; this indicates that the electrical transport in these films is controlled by the variation in the carrier's mobility rather than by their concentration.

The obtained values are in good agreement with that reported in the literature; Gremenok et al. and Neumann et al. have reported, respectively, the values ranging between 0.1 and 0.01 Ω cm for the electrical resistivity [15] and 6.99×10^{15} cm^{-3} for the carrier density [26]. Zhuze et al. reported room-temperature conductivity for p-type polycrystalline samples of the order of 5×10^{-3} Ω cm [27].

The Raman spectra of $CuInTe_2$ were recorded at room temperature in the range of 100–200 cm^{-1} using 532 nm argon-ion laser line as irradiator source. Figure 10a–d shows the Raman spectra of $CuInTe_2$ electrodeposited at different times. The green and the red lines denote the individual Lorentzian fit. Based on the two works of Rincon et al. [28, 29], the peaks positions and their assigned modes are discussed in bellow.

All the Raman spectra show up the line centered at 127 cm^{-1}; it is the most intense and narrowest for the films deposited at 5 and 15 min. This line is attributed to the A_1 mode which is the strongest line generally observed in the Raman spectra of the chalcopyrite structures. The A_1 mode originates from the motion of tellurium atom with copper and indium atoms remaining at rest. This mode is also observed at 123 cm^{-1} as reported by Prabukanthan and Lakhe and their coworkers [7, 30]. The peak located at 113 cm^{-1} is assigned to B_1^2 mode. The two lines centered at 105 and 145–148 cm^{-1} are assigned, respectively, to the B_2^2 and B_1^3 modes, the B_1^3 mode originates due to anti-phase motion of In and Cu [7]. The peak located at 139–141 cm^{-1} is attributed to the E^3 (LO) mode and the line at 160 cm^{-1} is assigned to the E^4 (TO) and (LO) modes. The line at 170 cm^{-1} is also observed by Murali et al. [21] and is assigned to the E^5 and/or the B_2^3 (TO) modes. The peak centered at 176 cm^{-1} is caused by the B_2 (TO) and/or E (TO) mode [31]. The line at 182–186 cm^{-1} is assigned to the E^5 and/or the B_2^3 (LO) modes. The peak centered at 192 cm^{-1} is assigned to the E^6 (TO) mode. The line at 120 cm^{-1} is also observed by several authors [31, 32], and is assigned to the Te atoms.

In addition, three weak peaks situated at 153, 157 and 167 cm^{-1} are observed in the Raman spectra of the films deposited at 15 and 20 min. These modes are reported to be due to In_4Te_3 secondary phase, although this phase is observed in X-ray diffraction pattern for these two films.

From the above results we have found that the film deposited during 10 min presents single phase, polycrystalline

Table 1 Room temperature values of carrier mobility, carrier concentration and the conductivity type for $CuInTe_2$ films

Deposition time (min)	Mobility ($cm^2\,V^{-1}\,s^{-1}$)	Conduction type	Carrier density (cm^{-3})
5	165	n	2.47×10^{15}
10	89.8	p	3.79×10^{15}
15	579	n	9.35×10^{14}
20	2.44×10^{6}	n	2.51×10^{11}

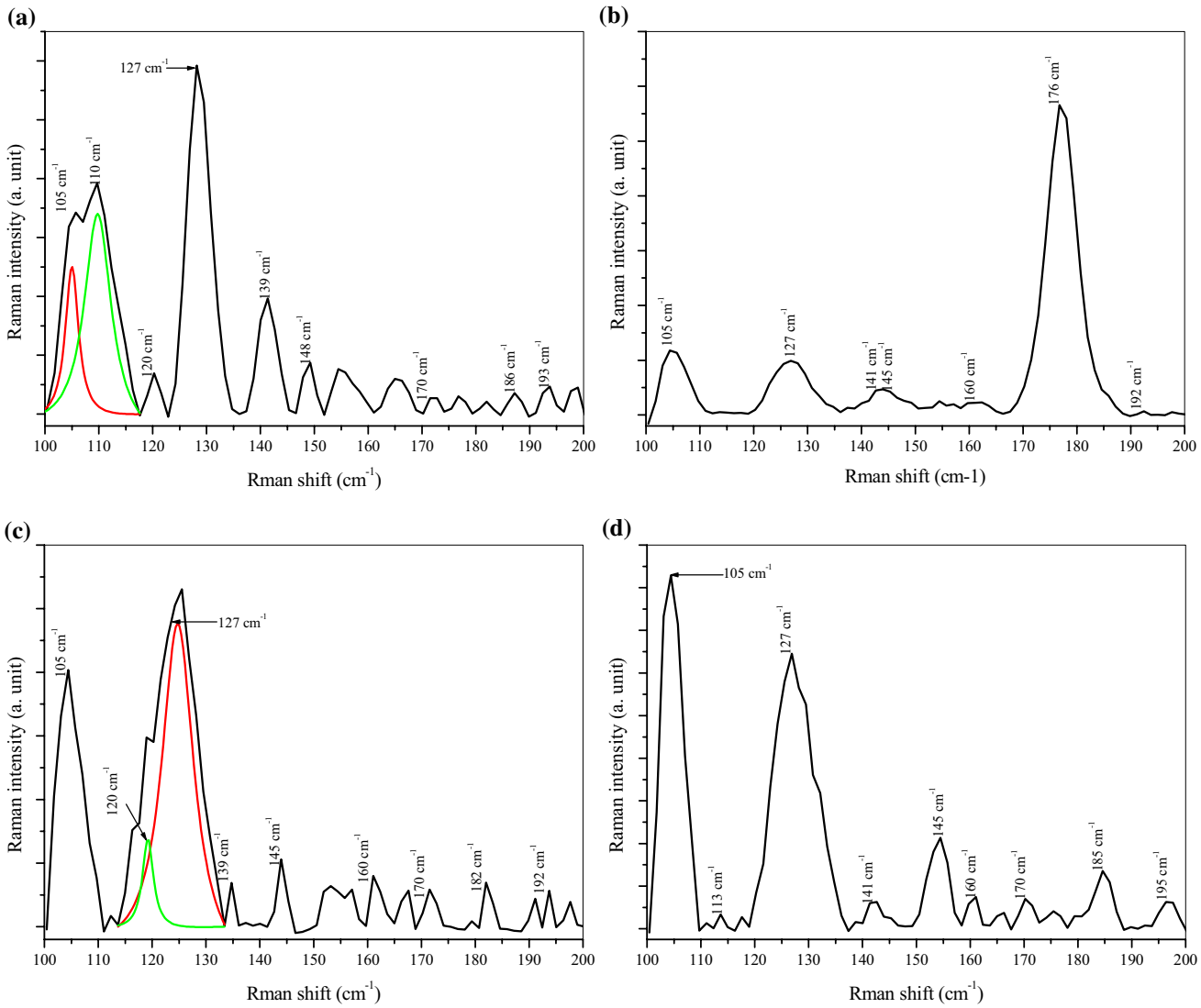

Fig. 10 Raman spectra of $CuInTe_2$ thin films deposited at different times; **a** 5, **b** 10, **c** 15 and **d** 20 min. The green and the red lines denote the individual Lorentzian fit

and chalcopyrite $CuInTe_2$ and exhibits better crystallinity and excellent optical properties, it can be used as a good absorber layer in the fabrication of thin film solar cells.

4 Conclusion

In the present work $CuInTe_2$ thin films were deposited on ITO-coated glass substrate using one-step electrodeposition process. The X-ray diffraction results indicate that the films deposited during 5 and 10 min exhibit a single phase chalcopyrite $CuInTe_2$ with a highly preferred [112] orientation, resulting in the improvement of crystalline quality. However, the films deposited during 15 and 20 min have the chalcopyrite structure as the major $CuInTe_2$ phase with a characteristic reflection from In_4Te_3 as a secondary phase.

The orthorhombic In_4Te_3 secondary phase gradually increases with deposition time. The obtained grain size values are ranged between 150 and 300 Å. The films surface morphology changes with deposition time. Hall effect measurements indicate that the film deposited during 10 min has p-type conduction. These results proved the interesting potential of electrodeposition as technique for the preparation of high quality and low cost $CuInTe_2$. The obtained films can be used as absorbing layer in thin film solar cells.

References

1. A.L. Dawar, A. Kumar, R.P. Mall, P.C. Mathur, Growth and electrical transport properties of $CuInTe_2$ thin films. Thin Solid Films **112**(84), 107–119 (1984). https://doi.org/10.1016/0040-6090(84)90488-7
2. P. Jackson, D. Hariskos, R. Wuerz, W. Wischmann, M. Powalla, Compositional investigation of potassium doped Cu(In,Ga) Se_2 solar cells with efficiencies up to 20.8%. Phys. Status Solidi Rapid Res. Lett. (RRL) **8**, 219–222 (2014). https://doi.org/10.1002/pssr.201409040
3. M. Lakhe, S.K. Mahapatra, N.B. Chaure, Development of $CuInTe_2$ thin film solar cells by electrochemical route with low temperature (80 °C) heat treatment procedure. Mater. Sci. Eng. B **204**, 20–26 (2016). https://doi.org/10.1016/j.mseb.2015.11.005
4. G.E.A. Muftah, A.P. Samantilleke, P.D. Warren, S.N. Heavens, I.M. Dharmadasa, Electrochemical deposition of $CuInTe_2$ layers for applications in thin film solar cells. J. Mater. Sci. Mater. Electron. **21**, 373–379 (2010). https://doi.org/10.1007/s10854-009-9926-z
5. T. Mise, T. Nakada, Low temperature growth and properties of Cu–In–Te based thin films for narrow bandgap solar cells. Thin Solid Films **518**, 5604–5609 (2010). https://doi.org/10.1016/j.tsf.2010.04.065
6. T. Mise, T. Nakada, Narrow-bandgap $CuIn_3Te_5$ thin-film solar cells, Prog. Photovolt Res. Appl. **21**, 754–759 (2011). https://doi.org/10.1002/pip.1191
7. M. Lakhe, N.B. Chaure, Characterization of electrochemically deposited $CuInTe_2$ thin films for solar cell applications. Sol. Energy Mater. Sol. Cells **123**, 122–129 (2014). https://doi.org/10.1016/j.solmat.2014.01.008
8. W. Horig, H. Neumann, V. Savelev, V. Lagzdonis, B. Schuhmann, G. Kiihn, Optical properties of flash-evaporated $CuInTe_2$ thin films. Cryst. Res. Technol. **24**, 823–827 (1989). https://doi.org/10.1002/crat.2170240819
9. M.J. Thwaites, R.D. Tomlinson, M.J. Hampshire, The observation of optical transitions from valence band states in $CuInTe_2$. Phys. Status Solidi (b) **94**, 211–214. (1979). https://doi.org/10.1002/pssb.2220940123
10. T. Ishizaki, N. Saito, A. Fuwa, Electrodeposition of $CuInTe_2$ film from an acidic solution. Surf. Coat. Technol. **182**, 156–160 (2004). https://doi.org/10.1016/j.surfcoat.2003.07.004
11. M.R. Ananthan, S. Kasiviswanaathan, Growth and characterization of stepwise flash evaporated $CuInTe_2$ thin films. Sol. Energy Mater. Sol. Cells **93**, 188–192 (2009). https://doi.org/10.1016/j.solmat.2008.09.024
12. C.D. Lokhande, S.H. Pawar, Electrodeposition of $CuInTe_2$ films. J. Phys. D Appl. Phys. **20**, 1213–1214 (1987). https://doi.org/10.1088/0022-3727/20/9/023
13. V.F. Gremenok, I.A. Victorov, I.V. Boudnar, A.E. Hill, R.D. Pikington, R.D. Tomlinson, M.V. Yakushev, Characterization of $CuInTe_2$ thin films prepared by pulsed laser deposition. Mater. Lett. **35**, 130–134 (1998). https://doi.org/10.1016/S0167-577X(97)00236-X
14. A. Bouraiou, M.S. Aida, O. Meglali, N. Attaf, Potential effect on the properties of $CuInSe_2$ thin films deposited using two-electrode system. Curr. Appl. Phys. **11**, 1173–1178 (2011). https://doi.org/10.1016/j.cap.2011.02.014
15. B.D. Cullity, *Elements of X-Ray Diffraction* (Addison-Wesley, Reading, 1956)
16. T. Mise, T. Nakada, Effect of tellurium deposition rate on the properties of Cu–In–Te based thin films and solar cells. J. Cryst. Growth **314**, 76–80 (2011). https://doi.org/10.1016/j.jcrysgro.2010.10.147
17. M. Boustani, K. El Assali, T. Bekkay, E. Ech-Chamikh, A. Outzourhit, A. Khiara, L. Dreesen, Characterization of $CuInTe_2$ thin films prepared by flash evaporation. Semicond. Sci. Technol. **12**, 1658–1661 (1997). https://doi.org/10.1088/0268-1242/12/12/020
18. M. Boustani, K.E.1 Assali, T. Bekkay, A. Khiara, Structural and optical properties of $CuInTe_2$ films prepared by thermal vacuum evaporation from a single source. Sol. Energy Mater. Sol. Cells **45**, 369–376 (1997). https://doi.org/10.1016/S0927-0248(96)00084-0
19. K.S. Knight, The crystal structures of $CuInSe_2$ and $CuInTe_2$. Mater. Res. Bull. **27**, 161–167 (1992). https://doi.org/10.1016/0025-5408(92)90209-I
20. A.S. Kindyak, V.V. Kindyak, Y.J. Latushko, Optical transitions in thin $CuIn(Te,Se)_2$ films near the fundamental absorption edge. Mater. Lett. **34**, 237–240 (1998). https://doi.org/10.1016/S0167-577X(97)00174-2
21. S.M. Wasim, A. Lacruz Vielma, C. Rincon, Optical absorption study of $CuInTe_2$ crystals grown from near-stoichiometric compositions. Solid State Commun. **51**, 935–937 (1984). https://doi.org/10.1016/0038-1098(84)90356-9
22. C. Kim, D.H. Kim, Y.S. Son, H. Kim, J.Y. Bae, Y.S. Han, Solvothermal synthesis and characterization of a $CuInTe_2$ absorber for thin-film photovoltaics. Mater. Res. Bull. **47**, 4054–4058 (2012). https://doi.org/10.1016/j.materresbull.2012.08.061
23. K.R. Murali, C. Vinothini, K. Srinivasan, Characteristics of pulse plated copper indium telluride films. Mater. Sci. Semicond. Proc. **15**, 194–198 (2012). https://doi.org/10.1016/j.mssp.2012.02.006
24. A. Lacruz, C. Rincon, G. Sanchez Pérez, S.M. Wasim, Electrical and optical properties of $CuInTe_2$ grown from near-stoichiometric compositions. Prog. Cryst. Growth Charact. **10**, 283–287 (1984). https://doi.org/10.1016/0146-3535(84)90046-7
25. S.M. Wasim, G. Sanchez Porras, H. Neumann, Electrical properties of $CuInTe_2$ single crystals annealed in an indium atmosphere. Solid State Commun. **54**, 239–240 (1985). https://doi.org/10.1016/0038-1098(85)91074-9
26. H. Neumann, B. Perlt, W. Horig, The optical properties of $CuInTe_2$ epitaxial layers. Thin Solid Films **182**, 115–119 (1989). https://doi.org/10.1016/0040-6090(89)90249-6
27. L.L. Kazmerski, Y.J. Juang, Vacuum-deposited $CuInTe_2$ thin films: growth, structural, and electrical properties. J. Vac. Sci. Technol. **14**, 769–776 (1977). https://doi.org/10.1116/1.569265
28. C. Rincon, S.M. Wassim, G. Marin, Raman spectra of the chalcopyrite compound $CuInTe_2$. J. Appl. Phys. **85**, 3925–3927 (1999). https://doi.org/10.1063/1.369767
29. C. Rincon, S.M. Wassim, G. Marin, Raman spectra of $CuInTe_2$, $CuIn_3Te_5$, and $CuIn_5Te_8$ ternary compounds. J. Appl. Phys. **88**, 3439–3444 (2000). https://doi.org/10.1063/1.1289225
30. P. Prabukanthan, R. Dhanasekaran, Growth of $CuInTe_2$ single crystals by iodine transport and their characterization. Mater. Res. Bull. **43**, 1996–2004 (2008). https://doi.org/10.1016/j.materresbull.2007.10.004
31. T. Mise, T. Nakada, Influence of copper to indium atomic ratio on the properties of Cu–In–Te based thin-film solar cells prepared by low-temperature co-evaporation. J. Vac. Sci. Technol. A **30**, 0512202 (2012). https://doi.org/10.1116/1.4736948
32. M.R. Ananthan, P. Malar, T. Osipowicz, S. Kasiviswanathan, Studies on interface between In_2O_3 and $CuInTe_2$ thin films. Appl. Surf. Sci. **418**, 388–392 (2017). https://doi.org/10.1016/j.apsusc.2016.12.124